Pulse shaping for on-demand emission of single Raman photons from a quantum-dot biexciton

Tom Praschan,[1] Dirk Heinze,[1] Dominik Breddermann,[1] Artur Zrenner,[1] Andrea Walther,[2] and Stefan Schumacher[1,3]

[1]*Department of Physics and Center for Optoelectronics and Photonics Paderborn (CeOPP), Paderborn University, Warburger Strasse 100, 33098 Paderborn, Germany*

[2]*Department of Mathematics, Humboldt-Universität zu Berlin, Unter den Linden 6, 10099 Berlin, Germany*

[3]*Wyant College of Optical Sciences, University of Arizona, Tucson, Arizona 85721, USA*

(Received 28 January 2021; revised 29 November 2021; accepted 1 December 2021; published 6 January 2022)

Semiconductor quantum dots embedded in optical cavities are promising on-demand sources of single photons. Here, we theoretically study single photon emission from an optically driven two-photon Raman transition between the biexciton and the ground state of a quantum dot. The advantage of this process is that it allows all-optical control of the properties of the emitted single photon with a laser pulse. However, with the presence of other decay channels and excitation-induced quantum interference, on-demand emission of the single Raman photon is generally difficult to achieve. Here we show that laser pulses with nontrivial shapes can be used to maintain excitation conditions for which, with increasing pulse intensities, the on-demand regime is reached. To provide a realistic picture of the achievable system performance, we include phonon-mediated processes in the theoretical calculations. While preserving both high photon purity and indistinguishability, we find that although based on a higher-order emission process, for realistic system parameters on-demand Raman photon emission is indeed achievable with suitably tailored laser pulses.

DOI: 10.1103/PhysRevB.105.045302

I. INTRODUCTION

Single-photon sources based on semiconductor quantum-dot systems are considered key components for integration into quantum computers [1] and quantum cryptographic applications [2]. These sources have to produce light with extraordinary quantum properties such as high indistinguishability, emission efficiency, and purity [3–9]. They are typically based on single-photon transitions from one quantum dot state to another or the cascaded emission of photons from a higher electronic configuration in a quantum dot. Basic properties of the emitted photons such as polarization state and frequency are often predetermined by the chosen quantum-dot transitions and structure used. Active control is difficult to achieve. Here, we use a different approach and consider a direct two-photon transition between the quantum-dot ground state and the biexciton state, which offers flexibility in the initial biexciton state preparation [10,11] with fidelities close to one and the emission of quantum light with up to two photons [12–14]. Previously, we demonstrated that the direct (nonlinear) two-photon emission process from the biexciton cannot only be used to emit a pair of photons but through a photonic Raman process also to emit a single photon with optical control [15,16]. The Raman emission process has the unique advantage that properties of the emitted photon can be controlled optically by the control laser, whereas they would otherwise be predetermined by the quantum-dot system [17]. As depicted in Fig. 1, a coherent control pulse drives the system from an occupied biexciton state into an intermediate virtual state inside the band gap from which the system then relaxes into its ground state by emitting a single photon [15]. This process was recently observed experimentally [18]. The single-photon emission can be enhanced using an optical cavity. Related types of optical Raman processes which allow at least partial optical control of the properties of the emitted photon, such as polarization state and frequency, were previously studied in detail in different three-level systems [15,19–23].

To unlock the full potential of quantum applications, high single-photon emission probabilities are required, exceeding 66% for linear quantum computing [24] and 50% for Boson sampling [25]. These numbers are based on a joint emission, transmission, and detection efficiency as discussed in Ref. [17]. For the single-photon emission of interest in the present paper, we have previously shown that the Raman resonance condition nontrivially depends on the shape of the control pulse triggering the emission [16,23]. Moreover, the Raman process can also act as a source of excitation-induced quantum interference instead of as a source of single-photon emission [23]. These two aspects play an increasingly important role for elevated control pulse intensities and generally tend to undermine our quest for entering the on-demand regime for single Raman photon generation.

In the present paper, we demonstrate that a systematically optimized pulse can be used to steer the emission into the desired single-photon channel and effectively suppress undesired emission and quantum paths in the system dynamics. In Figs. 1(c) and 1(d), we show a sample result for which a simple Gaussian pulse stimulates a single Raman photon emission into the cavity mode with energy $\hbar\omega_c$ (parameters of the Gaussian pulse were optimized to achieve maximum emission probability). Further optimization can then only be obtained using a nontrivial control pulse that does not

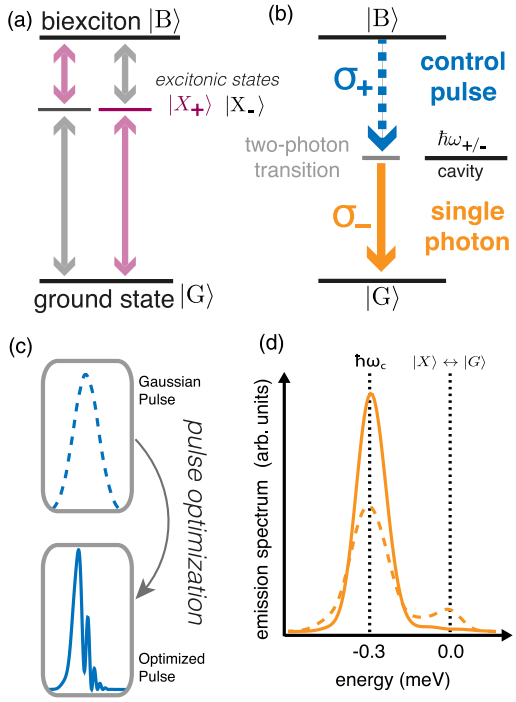

FIG. 1. (a) Sketch of the optical transitions in a semiconductor quantum dot in the circular polarization basis. (b) Sketch of the single-photon Raman emission process from a direct two-photon transition between biexciton and ground state. A control pulse with σ_+ circular polarization is used to stimulate the system into a virtual state, from which a single photon with σ_- circular polarization is then emitted as the system relaxes to its ground state. An optical cavity is used to enhance the single photon emission. In the present paper, using a mask in Fourier-space, systematically optimized control pulses are used to maximize the single-photon emission probability. An example of the pulse optimization in shown in (c). (d) Sample emission spectrum with (solid line) and without (dashed line) control pulse optimization. Optimization, in particular, decreases the emission into competing decay channels through the biexciton exciton cascade.

only enhance the Raman single photon emission probability significantly but also reduces competing emission channels. On a more detailed level, it is also important to note that the Raman single-photon emission benefits from resonance enhancement when occurring spectrally close to the dipole-allowed quantum dot transitions. However, with the cavity mode nearby these transitions, cavity feeding assisted by longitudinal acoustic (LA) phonons also becomes important. We show that even including these additional processes, for realistic system parameters and using well-established and experimentally accessible methods of pulse shaping, the on-demand regime for emission of single Raman photons from a quantum-dot cavity system can indeed be reached while preserving important figures of merit such as indistinguishability and single-photon purity.

In the following section, Sec. II, we briefly introduce the quantum dot cavity model used in the calculations. We describe the theory in more detail in Appendix A. In Sec. III, we present our method of optimizing the single-photon emission. We do this by introducing the theoretical concept of a Raman population which we then optimize systematically using shaped pulses. In Sec. IV, we discuss the results in the weak and strong coupling regimes.

II. QUANTUM DOT SYSTEM AND ITS PROPERTIES

We model the quantum dot by including the relevant electronic configurations which are the ground state $|G\rangle$, two excitons $|X_H\rangle$ and $|X_V\rangle$, and the biexciton state $|B\rangle$, with respective energies E_G, $E_{H,V}$, and E_B. We also include two degenerate cavity modes with frequencies $\omega_{H,V}$ and polarizations that correspond to those of the excitons. We describe the coupling of the cavity modes to the electronic transitions with a coupling constant g and add a coupling to a classical light field ($\sim\Omega_i$), which is discussed in detail in Sec. III B. To trigger the single photon Raman emission, we use a circularly polarized pulse; the desired single photon emission can then be detected in the other circular polarization channel as sketched in Fig. 1. In the circularly polarized frame, the coherent light field and cavity photon operators take the following form: $\Omega^*_{\sigma^\pm} = \frac{1}{\sqrt{2}}(\Omega^*_H \pm i\Omega^*_V)$ and $b^\dagger_{\sigma^\pm} = \frac{1}{\sqrt{2}}(b^\dagger_H \pm i b^\dagger_V)$. We assume zero fine-structure splitting for the excitons ($\delta_{\text{fss}} = 0$), such that the circular states are electronic eigenstates of the quantum dot system. However, we note that the single photon emission studied does not depend on this specific choice; quantitative changes for the Raman emission would be negligible [15] for typical values of δ_{fss} [26] for the pulse and cavity detunings discussed here. The system dynamics is calculated by solving the Liouville-von Neuman equation in matrix representation which is outlined in Appendix A 2. We consider coupling of the quantum dot system to a bath of LA phonons (see Appendix A 1 b) and apply a polaron transformation (see Appendix A 1 c) to obtain the relevant equations of motion in the polaron frame. In this approach, the phonon-assisted transitions are included as Lindblad-type contributions to the system dynamics. This allows us to introduce and optimize the analytical Raman emission probability as detailed in Sec. III A. This would not be straightforward with the numerically exact path integral treatment of the phonons [27–29] that has recently gained attention. Consequently, in the present paper we restrict our analysis to the limiting cases in which the Lindblad terms describe the phonon interaction well [30] as discussed in more detail below. We also include cavity losses, with a rate κ that is varied as needed to account for weak and strong coupling. Additionally, we include losses into other noncavity modes with a decay rate of $\gamma_{\text{rad}} = 2\,\mu\text{eV}$ in our calculations. Furthermore, we add a pure dephasing term that goes beyond phonon-assisted transitions [31] and which at low temperatures T scales linearly $\gamma_{\text{pure}}(T) = {}^{1\mu\text{eV}}/_{K} \times T$ [32]. By applying the quantum regression theorem, photon properties are calculated from two-time expectation values such as the emission spectrum, indistinguishability, and purity of the emitted single photon (a more detailed account is given in Appendix A 3).

III. SINGLE PHOTON EMISSION OPTIMIZATION

Single-photon sources with a high emission probability or brightness are a desired key component for future quantum applications. Therefore, it is crucial to improve the single photon output of such sources. In this paper, we consider

a single-photon emission process based on the stimulated emission from a biexciton state in a quantum dot, as outlined in the Introduction. However, there also exist different competing spontaneous decay channels. Thus, it is necessary to isolate the contribution of the desired, triggered single-photon emission in the optimization process. To this end, in Sec. III A below we introduce the single-photon Raman emission probability which is then used to optimize the source's brightness. This optimization then results in an optimized optical control pulse that triggers the Raman photon emission process with its maximum yield. We parametrize the pulse in an experimentally accessible way based on well-established pulse-shaping technology as detailed in Sec. III B, with additional remarks concerning the optimization in Sec. III C.

A. Raman population

We are interested in the photon emission of the quantum light source. The total photon emission probability from the optical cavity with photon polarization i during a time span $\mathcal{T}$ is given by [33]

$$\mathcal{P}_{\mathrm{ems},i}(\mathcal{T}) = \kappa \int_0^{\mathcal{T}} N_i(t)\, dt, \tag{1}$$

where κ is the cavity decay rate and $N_i(t) = \mathrm{tr}(\rho(t)\, b_i^\dagger b_i)$ is the photon population. This expression combines all photons from different decay/emission events. We are, however, only interested in the emission of a certain photon from the optically controlled, direct transition from the biexciton to the ground state. Following Ref. [23], we introduce the single-photon Raman emission probability of polarization i as

$$\mathcal{P}_{\mathcal{R},i}(\mathcal{T}) = \kappa \int_0^{\mathcal{T}} N_{\mathcal{R},i}(t)\, dt. \tag{2}$$

Here, we are interested in the circularly polarized population of the Raman photon $N_{\mathcal{R},\sigma_-}(t)$. This is obtained from the Heisenberg equation for the mean of the circularly polarized cavity photon number operator up to second order in the hierarchy with the Raman process:

$$\mathcal{R}_{\sigma_-}(t) = \langle |G\rangle\langle B| b^\dagger_{\sigma-}(t)\Omega^*_{\sigma_+}(t)\rangle. \tag{3}$$

This describes the Raman process where the quantum dot transition from the biexciton $\langle B|$ to the ground state $|G\rangle$ is triggered by a σ_+ polarized control pulse $\Omega^*_{\sigma_+}(t)$ and, consequently, a single photon of opposite polarization $b^\dagger_{\sigma-}(t)$ is created in the cavity mode. Integrating the second-order equation while keeping only the terms proportional to the Raman process yields

$$\begin{aligned} N_{\mathcal{R},\sigma_-}(t) = \frac{2g\langle B\rangle^2}{\hbar^2}\,\mathrm{Re}\int_0^t\int_0^{t'} & e^{-\kappa(t-t')} \\ & \times (e^{W_{BX}(t')-W_{BX}(t'')} - e^{W_{XG}(t')-W_{XG}(t'')}) \\ & \times \mathcal{R}_{\sigma_-}(t'')\, dt''\, dt', \end{aligned} \tag{4}$$

where we have $W_{\alpha\beta}(t) = -\mathrm{i}\int_0^t \omega_{\alpha\beta,c}(t')\, dt'$, and $\omega_{\alpha\beta,c}(t) := \omega_\alpha - \omega_\beta - \omega_c - \frac{\mathrm{i}}{2}(\kappa + \bar{\Gamma}_{\alpha\beta}(t))$, with $\omega_{\alpha/\beta}$ relating to the quantum-dot energies, and $\hbar\omega_c$ is the energy of the cavity mode. The quantum-dot decay terms read

$$\bar{\Gamma}_{X_{\sigma-}G}(t) = \Gamma_{XG} + \Gamma^{X_{\sigma+}G}_{L,+}(t) + \Gamma^{BX_{\sigma-}}_{L,+}(t), \tag{5}$$

$$\bar{\Gamma}_{BX_{\sigma+}}(t) = \Gamma_{BX} + \Gamma^{GX_{\sigma+}}_{L,-}(t) + \Gamma^{X_{\sigma-}B}_{L,-}(t). \tag{6}$$

The pure dephasing and radiative decay are included via $\Gamma_{XG} = \gamma_{\mathrm{pure}} + \gamma_{\mathrm{rad}}$ and $\Gamma_{BX} = \gamma_{\mathrm{pure}} + 3\gamma_{\mathrm{rad}}$ [16] while the phonon-mediated processes driven by the laser field $\Gamma^{\alpha/\beta}_{L,\pm}$ are approximated by the analytical rates from Refs. [30,34]. We neglect the cavity photon mediated rates as $\langle B\rangle^2 g^2 \ll \kappa$ in our case. When we consider the single-photon emission without the phonon-assisted processes, we set $\langle B\rangle = 1$ and $\bar{\Gamma}_{\alpha\beta}(t) = \Gamma_{\alpha\beta}$.

B. Pulse shaping

We model the pulse shaping required for the numerical optimization according to the output of a $4-f$ pulse shaper [35]. Here, an input beam is focused onto a spatial light modulator (SLM), which makes it possible to introduce a frequency-dependent phase. The SLM applies a mask M to an input field Ω^{in} in frequency domain

$$\Omega^{\mathrm{SLM}}(\omega) = M(\omega)\Omega^{\mathrm{in}}(\omega), \tag{7}$$

with $M(\omega) = A_M(\omega)e^{i\phi_M(\omega)}$. A common choice is to set $A_M(\omega) = 1$, which implies that the pulse intensity will be preserved by the SLM [36]. The phase mask is given by

$$\phi_M(\omega) = \alpha\cos[2\pi\gamma(\omega-\omega_L)+\delta] + \eta(\omega-\omega_L)^2. \tag{8}$$

The first term models a periodic phase commonly used in optimal quantum control [37]. The second term is a quadratic phase which introduces a linear chirp in the time domain [38] and which is used to account for pulse-induced shifts during the single-photon emission process. These shifts are a major contribution to the overall pulse shape and can be analytically understood in the context of Raman emission from three-level systems (cf. footnote Ref. [45] of Ref. [23]). We choose a Gaussian-shaped input field

$$\Omega^{\mathrm{in}}_{\sigma+}(t) = \hbar\sqrt{\frac{\mathcal{E}_0\pi}{4\ \mathrm{ps}\ \sigma}}e^{-(\frac{t-t_0}{\sigma})^2}e^{i\omega_L t} \ \text{ and } \ \Omega^{\mathrm{in}}_{\sigma-}(t) = 0, \tag{9}$$

with pulse width σ, center t_0, dimensionless measure of energy $\mathcal{E}_0$, and $\hbar\omega_L = E_B - E_G - \hbar\omega_C + \Delta_L$, where Δ_L is a small detuning accounting for pulse-induced resonance shifts. The pulse-shaping method conserves the pulse energy, hence the dimensionless amplitude $\mathcal{E}_0$ acts as a constraint for the optimized pulse.

C. Optimizing the single photon emission

We aim to optimize the single-photon emission as quantified by the Raman emission probability $\mathcal{P}_{\mathcal{R},\sigma-}$ in Eq. (2). The parametrization of the pulse as introduced in the previous section leads to a seven-dimensional optimization problem with parameters $x = \{\alpha, \gamma, \delta, \eta, \sigma, t_0, \Delta_L\}$. In this space, we numerically seek [39]

$$\max_x\ \mathcal{P}_{\mathcal{R},\sigma-}(x). \tag{10}$$

We restrict the set x to parameters suitable for common SLMs and chirped pulses based on Refs. [40,41] with

$$0 \leqslant \alpha \leqslant 2\pi, \quad 0\ \text{meV}^{-1} \leqslant \gamma \leqslant 2\ \text{meV}^{-1},$$
$$0 \leqslant \delta \leqslant 2\pi, \quad -25\ \text{meV}^{-2} \leqslant \eta \leqslant 25\ \text{meV}^{-2},$$
$$15\ \text{ps} \leqslant t_0 \leqslant 30\ \text{ps}, \quad 2.5\ \text{ps} \leqslant \sigma \leqslant 5\ \text{ps}.$$

A (strong) external light field coupled to the quantum dot system changes the transition energies of the quantum dot. The shift for the transition of interest, which in general depends on time, can be calculated analytically in some limiting cases [23]. The most important observation is that the shift of the resonance can be well approximated by a linear chirp in the time domain, η. Additionally, we include control of the pulse frequency components with the parameters α, γ, δ, which will steer the pulse energy into the desired spectral regions and away from regions which will contribute to unwanted quantum interference [23]. Furthermore, we consider an average laser detuning Δ_L [15], which is the simplest way to optimize by hand. We note that for large pulse detuning from the electronic resonances and a strong pulse inclusion of the average detuning alone, Δ_L can already yield a significant improvement in the photon population gained [15]. Lastly, we allow slight variations in the pulse width with σ and pulse maximum with t_0.

The numerical optimization of the single-photon Raman emission probability is performed by applying advanced nonlinear optimization algorithms as implemented in the IPOPT (INTERIOR POINT OPTIMIZER) software package [42–44]. This requires the numerical evaluation of both the gradient and the Hessian matrix of the circular Raman emission. To calculate the occurring partial derivatives with machine precision, we employ *algorithmic differentiation* (AD) [45–48]. The CoDiPack library [49] is used for AD as it shows a high performance for the problem considered in this paper. We employ forward-mode AD which is more efficient than reverse mode for the given number of optimization parameters and parallelize the computations of the partial derivatives.

IV. RESULTS AND DISCUSSION

In this section, we discuss the main results of the single photon Raman emission optimization. We begin the analysis in Sec. IV A with the unoptimized case. We carry on with Sec. IV B, where we study the Raman output depending on the cavity detuning in the weak optical coupling regime. In Sec. IV C, we examine the potential for on-demand operation for higher quality cavities approaching the strong coupling regime, while preserving other important photon properties such as indistinguishability and purity.

A. Unoptimized single photon emission

First, we look at the dependence of the single photon Raman emission on the detuning of a cavity mode in the weak optical coupling regime with $g/\kappa = 0.35$. We consider the case of an un-optimized ($\Omega^{\text{SLM}} = \Omega^{\text{in}}$) control pulse. In our simulations, we assume the initial condition that the quantum dot is prepared in the biexciton state and there are no photons in the cavity modes. The results are shown in Fig. 2 for

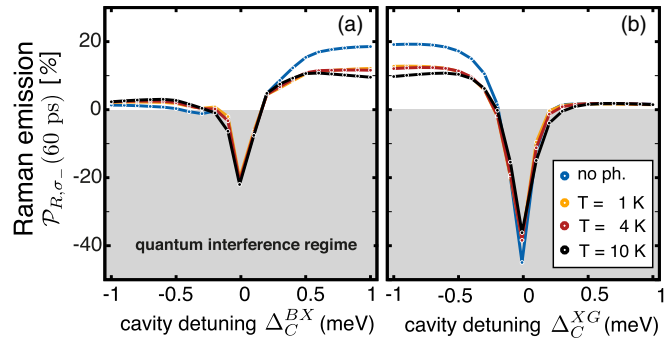

FIG. 2. Dependence of the unoptimized single-photon Raman emission probability on the detuning of the cavity from the biexciton to exciton transition $\Delta_C^{BX} = \hbar\omega_C - E_B + E_X$ in (a) and the exciton to ground-state transition $\Delta_C^{XG} = \hbar\omega_C - E_X$ in (b). Results are shown without any optimization for zero phonon coupling as well as for calculations including the phonon-assisted processes at temperatures $T = 1\,\text{K}$, $T = 4\,\text{K}$, and $T = 10\,\text{K}$ for $g/\kappa = 0.35$. We constrain the pulse optimization to $\mathcal{E}_0 = 4$. Negative values of the Raman emission probability indicate undesired quantum interference as discussed in the main text.

which we limited the pulse intensity to $\mathcal{E}_0 = 4$. The maximum Raman emission probability in this case does not exceed 20%. The strongest emission can be found between the two resonances where the Raman process benefits most from the resonance enhancement of both optically active transitions. If the cavity is tuned close to resonance with the electronic transitions, the Raman emission probability becomes negative, which indicates quantum interference of different photon-emission paths, diminishing the emission of the spontaneous cavity-enhanced decay of the electronic states, as discussed in more detail in Ref. [23].

Next, we consider strong coupling of the cavity mode to the electronic resonances with $g/\kappa = 1$. The two-photon transition can be driven at any energy. To observe a bright emission, the transition must be driven near the real (bi)excitonic transitions. Furthermore, the quality factor of the cavity hardly changes the energy of the maximum Raman emission and slight deviations can always be compensated by the control pulse. So, we choose the cavity mode to enhance the Raman emission at $\Delta_C^{BX/XG} = \pm 0.3$ meV for comparison with the optimized case later on according to Fig. 4. The results are presented in Fig. 3. With the cavity tuned close to the biexciton to exciton resonance, we observe that the Raman emission [Fig. 3(a)] is not only below 20% but also it is only a fraction of the total cavity emission [Fig. 3(b)]. Consequently, we do not observe a pure Raman photon in this case which is also reflected in the comparatively low degree of indistinguishably [Fig. 3(c)]. Tuning the cavity to $\Delta_C^{XG} = -0.3$ meV produces a similar picture. However, it can be seen that the total cavity emission [Fig. 3(e)] levels off at above 20% emission probability while the Raman emission [Fig. 3(d)] decreases. Therefore, the observed total emission probability has to be produced by alternative (non-Raman) emission processes which consequently revive the indistinguishability [Fig. 3(f)] at high pulse areas.

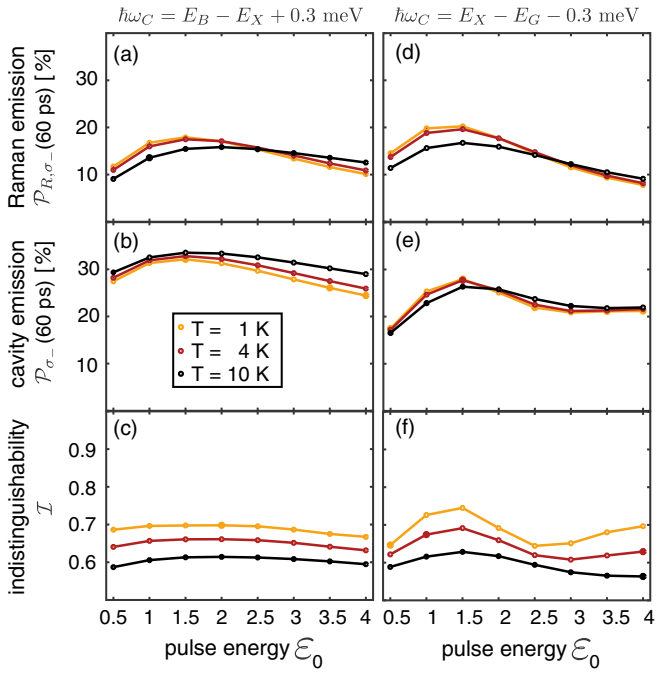

FIG. 3. Dependence of the unoptimized single-photon emission probability and indistinguishability on the control pulse strength. The influence of electron-phonon coupling is shown for the single-photon Raman emission probability [(a), (d)], the total cavity emission [(b), (e)], and the indistinguishability [(c), (f)], depending on the pulse strength for the two most promising cavity detunings from Fig. 2. However, here we consider a higher-Q cavity with $g = \kappa$ at $Q \approx 21\,000$.

Using simple Gaussian pulses does allow us to trigger single-photon emission from a quantum dot biexciton, however, the observed results are far from on-demand emission behavior and the desired process cannot be triggered exclusively. In the next sections, we demonstrate how pulse optimization makes on-demand single photon Raman emission possible.

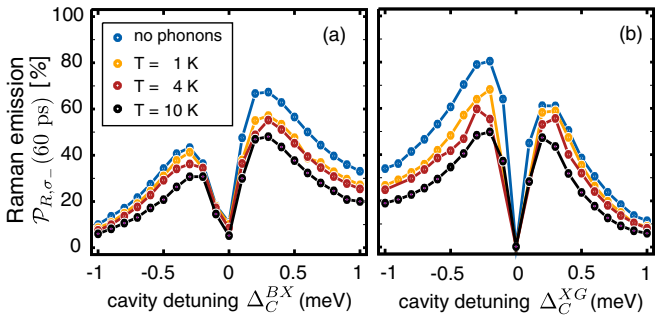

FIG. 4. Dependence of the single-photon Raman emission probability on the detuning of the cavity from the biexciton to exciton transition $\Delta_C^{BX} = \hbar\omega_C - E_B + E_X$ in (a) and the exciton to ground state transition $\Delta_C^{XG} = \hbar\omega_C - E_X$ in (b). Results are shown for zero phonon coupling as well as for calculations including the phonon-assisted processes at temperatures $T = 1$ K, $T = 4$ K, and $T = 10$ K for $g/\kappa = 0.35$ and $\mathcal{E}_0 = 4$.

B. Single photon Raman emission

In this section, we turn to study the emission of optimized Raman photons in a medium-Q cavity with $g/\kappa = 0.35$. We start by examining the dependence of the single-photon Raman emission depending on the detuning of the cavity mode from the closest nearby quantum-dot resonance. Just as above, we assume that at time $t = 0$ the quantum dot system is initialized in the biexciton state and no photons are present in the optical cavities. Figure 4 depicts the resulting Raman emission probability for optimized pulses that are constrained to the dimensionless pulse amplitude $\mathcal{E}_0 = 4$. Results are shown with phonon-mediated transitions at $T = 1$ K, $T = 4$ K, and $T = 10$ K as well as without phonon coupling for comparison. In the cases considered, the single-photon emission process is completed for times smaller than 60 ps. Spectrally approaching the single-photon resonances in the quantum dot system again leads to a resonance enhancement also in the nonlinear system response and enhances the emission probability of the single Raman photons. Exactly on resonance, however, at $\Delta_C^{BX/XG} = 0$, where one would expect the total cavity emission probability to peak (not shown in Fig. 4), the Raman emission rate also with optimization is close to zero due to quantum interference of different emission channels [23]. Nevertheless, in this case due to the optimization of the pulse, the Raman emission probability contributes positively to the overall emission. Again we observe the resonance enhancement from the nearby real transitions to be strongest if the cavity is positioned between the electronic quantum dot resonances, with a slight asymmetry favoring the exciton to ground-state transition. The strongest single Raman photon emission is found for detunings $\Delta_C^{BX/XG} = \pm 0.3$ meV. We note that to realistically benchmark the system dynamics this close to the resonance condition, phonon-mediated processes must be taken into account. Overall, we observe that the coupling to phonons reduces the single-photon emission probability. The phonon-assisted processes open alternative and competing decay channels and, in addition, $\langle B \rangle < 1$ directly reduces the generated Raman photon number average. At low temperatures, the phonon bath can more easily absorb than emit quanta of energy. Thus, phonon-assisted absorption and emission prefer opposite spectral detunings [50]. Phonon-assisted emission of a photon into the cavity mode occurs if $\Delta_C^{BX/XG} < 0$. In these cases, tuning the cavity to the biexciton to exciton resonance does only increase the background emission. If, however, the cavity is tuned to the exciton to ground-state transition, phonon-assisted transitions hinder the control laser to stimulate the higher order Raman process. Consequently, the Raman emission probability is decreased. On the other hand, if $\Delta_C^{BX/XG} > 0$ these effects are weak, but now the control laser is negatively detuned from the closest quantum-dot resonance so the laser may induce optical transitions via the phonon side bands. However, in the case of $\Delta_C^{XG} > 0$, the phonon interaction mainly introduces another decay path to the system. We find an overall low degree of second-order coherence of the emitted photons, with $g^{(2)}_{\sigma_-}(0)$ being well below 0.1.

We note that for a medium-quality cavity with $g/\kappa = 0.35$ or $Q = 7447$ at 880 nm we find that the Raman emission probability at low temperatures ($T = 4$ K) can reach

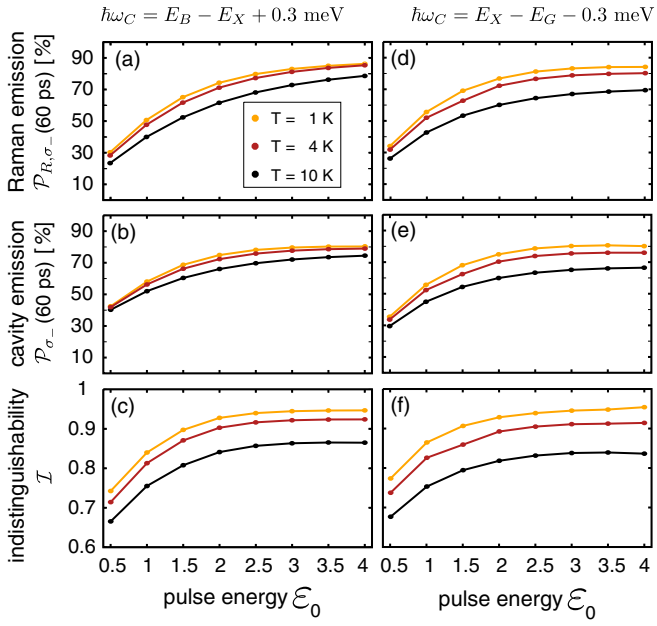

FIG. 5. Dependence of the single-photon emission probability and indistinguishability on the control pulse strength. The influence of electron-phonon coupling is shown for the single-photon Raman emission probability [(a), (d)], the total cavity emission [(b), (e)], and the indistinguishability [(c), (f)], depending on the pulse strength for the two most promising cavity detunings from Fig. 4. Here, a high-Q cavity with $g = \kappa$ at $Q \approx 21\,000$ is used.

60% and as such is already sufficient for quantum computing applications such as Boson sampling [25]. This is only possible by optimizing the pulse so it already includes the pulse-induced resonance shifts that alter the single-photon Raman transition as introduced in Sec. III C. Here, the pulse-optimized Raman emission completely avoids the undesired quantum interference regime and can produce sufficiently high degrees of emission probability close to the electronic transitions.

C. Single photon emission and properties

Above we only considered a medium-quality cavity which did not reach the required threshold of a photon emission probability of 2/3 for on-demand emission [24]. In the present section, we further increase the light-matter coupling in our analysis. Now, a high-Q cavity with $g = \kappa$ is used. In Fig. 5, we show the total photon emission probability of the σ_--polarized cavity mode, the Raman emission probability, and the indistinguishability of the photons after the optimization process. One sees that a single-photon emission probability can be reached that is now high enough to be considered on demand. The dependence of the single-photon Raman emission probability on the detuning of the cavity from the electronic transition is similar to the case of low exciton-cavity coupling in the previous section because a higher Q factor increases the photonic mode density at the desired frequency and thus increases the brightness of the source. We analyze the two situations most suitable for single-photon emission with $\Delta_C^{BX} = +0.3$ meV and $\Delta_C^{XG} = -0.3$ meV. Again, it is assumed that at time $t = 0$ the quantum dot system is initialized in the biexciton state and no photons are present in the optical cavity modes. With increasing pulse energy $\mathcal{E}_0$ the Raman emission and the total cavity emission rise. The higher light-matter coupling partly compensates for the detrimental influence of the electron-phonon coupling. In general, as the pulse energy increases, the phonon-assisted effects become more pronounced, since they scale with the square of the pulse energy as given in Eq. (A17). This leads to a saturation in achievable photon output at large pulse energies. We find a maximum Raman emission probability of $\mathcal{P}_{R,\sigma_-} \approx 85\,\%$ in the case of $\Delta_C^{BX} = +0.3$ meV and a slightly lower value of $\mathcal{P}_{R,\sigma_-} \approx 80\,\%$ for $\Delta_C^{XG} = -0.3$ meV at the typical experimental temperature of $T = 4$ K and $\mathcal{E}_0 = 4$. The difference $\mathcal{P}_{R,\sigma_-} - \mathcal{P}_{\sigma_-}$, which can be associated with destructive quantum interference [23], is marginal at high pulse energies, so the quantum light source can be characterized as an on-demand source with emission probabilities of ∼80 %. At higher temperatures of $T = 10$ K, the optimized emission probability still exceeds the on-demand limit for $\Delta_C^{BX} = +0.3$ meV. However, in the case of $\Delta_C^{XG} = -0.3$ meV, the emission probability is about 10% lower because, even in the case of a positively detuned laser from the biexciton to exciton transition, with increasing temperature the phonon bath is more likely to emit quanta of energy to bridge the energy gap Δ_C^{XG} for pulse-induced optical transitions.

In Figs. 5(c) and 5(f), we depict the calculated indistinguishabilities for both detunings. At first, the indistinguishability rises with increasing pulse amplitude $\mathcal{E}_0$ until it plateaus because of phonon-induced coupling. At higher temperatures, the indistinguishability is reduced for $\Delta_C^{XG} = -0.3$ meV in comparison with $\Delta_C^{BX} = +0.3$ meV. Here, starting with an occupied biexciton, the σ_+-polarized pulse can populate the $|X_-\rangle$ exciton with rising temperature more easily, resulting in the emission of σ_--polarized photons into the cavity mode, which consequently reduces the indistinguishability of the triggered σ_--polarized Raman photon. However, at low temperatures the phonon-mediated process is suppressed, allowing high values of $\mathcal{I} \approx 0.95$ at $T = 1$ K and $\mathcal{I} \approx 0.92$ at $T = 4$ K. Additionally, since the off-resonant high-Q cavity suppresses the (phonon-assisted) cascaded two-photon emission, an overall high single photon purity is found. While we observe the highest purity at the lowest temperature, we find a low degree of second order coherence $g^{(2)}_{\sigma_-}(0) < 0.01$ even at $T = 10$ K.

Optimizing the pulses for single-photon Raman emission allows for pure Raman emission at high pulse intensities. Consequently, the achieved indistinguishably is comparatively high. In Appendix B, we provide example parameters of the optimized pulses.

Lastly, we analyze the effect of the fidelity of the initially prepared biexciton state. As a rule of thumb, the figures of merit analyzed here scale down with the initial biexciton occupation. However, the specific numbers depend on the shape and arrival time of the pulse. As a simple example, here we look at the direct two-photon preparation that suffers from damping by phonons in contrast to preparation via the phonon sideband [51,52] and thus cannot be fully inverted. A comparison of different optical excitation schemes under the influence of phonons can be found in Ref. [53]. We note

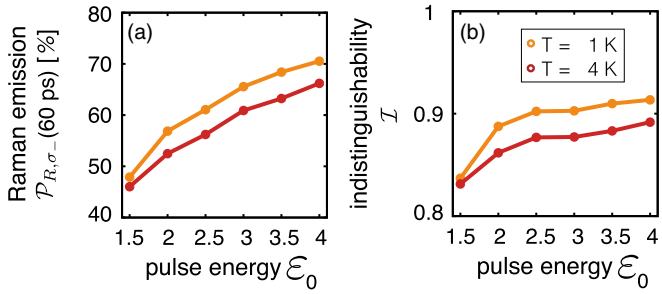

FIG. 6. Single-photon emission with optical biexciton initialization. A two-photon absorption process is used to prepare the biexciton state from the initial ground state $\rho(0) = |G\rangle\langle G|$ with a peak occupation of $N_B \approx 0.72$. Depicted are the single photon Raman emission probability (a) and the indistinguishability (b), depending on the strength of the control pulse for the case of $\Delta_C^{BX} = +0.3$ meV. Again, a high-Q cavity with $g = \kappa$ and $Q \approx 21000$ is used.

that the phonon-assisted preparation of the biexciton state suffers more from higher temperatures than other preparation protocols, as it is already reduced to about 50% at 40 K. So far, we have considered a maximum initial fidelity of $N_B(t_I = 0) = 1$, where $t_I \geqslant 0$ is the time when the maximum biexciton occupation is reached. To simulate the case of $N_B(t_i) < 1$, we use a Gaussian pulse to incompletely drive the system from the ground state ($\rho(0) = |G\rangle\langle G|$) into the biexciton state by two-photon absorption with a peak occupation of $N_B \approx 0.72$. In Fig. 6, we depict the Raman emission probability and the indistinguishability for $\Delta_C^{BX} = +0.3$ meV. It should be noted that the photon emission probabilities can exceed N_B because the decaying biexciton does emit two photons. The photon emission probabilities as well as the indistinguishability are reduced for all values of the pulse amplitude and temperature. The single photon purity decreases only slightly with the pulse amplitude as $g^{(2)}_{\sigma_-}(0) < 0.002$.

Although we find that almost all of the initial biexciton occupations can be used for the creation of a single Raman photon through the control pulse optimization, the quantum efficiency of the single photon source is limited by the fidelity of the initial biexciton occupation. We note that the latter can be optimized separately. However, even with significantly reduced initial biexciton occupation, we find on-demand single Raman photon emission from the biexciton within reach at low temperatures and sufficiently high pulse energies.

We also demonstrated the importance of pulse optimization. In the more complex partially stimulated two-photon emission process, the pulse itself changes the resonances of the system while it drives the Raman emission. This effect was first analyzed for different three-level systems [23]. Here, we expanded the analysis to the diamond-shaped four-level biexciton system and showed that the optimization of chirped pulses whose parameters are compatible with experimentally available SLMs is sufficient to achieve on-demand single-photon Raman emission from a quantum dot biexciton. This emission process has the advantage that single-photon properties can be controlled all-optically with the control laser and do not solely depend on the intrinsic quantum dot parameters.

V. CONCLUSION

We have studied the systematic optimization of a Raman single-photon source based on a partially stimulated two-photon emission process from the quantum dot biexciton inside an optical cavity. We find that the underlying Raman process is most efficient if the optical cavity used to enhance the light-matter coupling is placed near and between the electronic transitions of the quantum dot. We show that nontrivial shapes of the pulses triggering the Raman photon emission are key to suppressing competing emission mechanisms. For an initially fully populated biexciton state and a sufficiently high-Q cavity (here with $Q = 21\,000$ and $g = \kappa$), we numerically demonstrate single Raman photon emission with a probability of ∼80% and simultaneously high indistinguishability of ∼92% and high single-photon purity with $g^{(2)}(0) < 0.01$. Even with incomplete optical biexciton initialization, the on-demand regime can still be reached for realistic system parameters.

ACKNOWLEDGMENTS

This work was supported by the Deutsche Forschungsgemeinschaft (DFG) through the collaborative research center TRR142 (Grant No. 231447078, project A03) and Heisenberg program (Grant No. 270619725) and by the Paderborn Center for Parallel Computing, PC^2.

APPENDIX A: DETAILED THEORY

In this Appendix, we lay out the theory used to describe the nonlinear excitation dynamics in the quantum dot cavity system considered. In Appendix A 1, we introduce the system Hamiltonian which is used to calculate the system dynamics in Appendix A 2, including couplings to the environment. We then summarize how to calculate the single-photon emission spectra in Appendix A 3 a and photon indistinguishibility and purity in Appendix A 3 b.

1. Hamiltonian

The quantum dot cavity system outlined in Sec. II can be described with the Hamiltonian [31,54]

$$H = H_0 + H_S + H_{\mathrm{B}} + H_{\mathrm{QD-Ph}}, \tag{A1}$$

where H_0 and $H_S = H_{\mathrm{QD-Cav}} + H_{\mathrm{QD-L}}$ concern the QD-cavity system of which we give a detailed description in Appendix A 1 a. The Hamiltonian of the phonon bath H_{B} and its coupling to the quantum dot system are discussed in Appendix A 1 b.

a. Qunatum dot cavity part

We model the quantum dot by including the relevant electronic configurations which are the ground state $|G\rangle$, two excitons $|X_H\rangle$ and $|X_V\rangle$, and the biexciton state $|B\rangle$, with respective energies E_G, E_i, and E_B. We also include two degenerate cavity modes with frequencies $\omega_{H,V}$ and polarizations that correspond to those of the excitons. The free system

Hamiltonian then reads

$$H_0 = E_G|G\rangle\langle G| + E_B|B\rangle\langle B| + \sum_{i=H,V} (E_i|X_i\rangle\langle X_i| + \hbar\omega_i b_i^\dagger b_i). \quad \text{(A2)}$$

The electronic system couples to the cavity modes,

$$H_{\mathrm{QD-Cav}} = \sum_{i=H,V} (g(|G\rangle\langle X_i|b_i^\dagger + |X_i\rangle\langle B|b_i^\dagger) + \mathrm{H.c.}), \quad \text{(A3)}$$

with coupling strength g and cavity photon operators $b_i^{(\dagger)}$. To trigger the single-photon emission, we include an off-resonant coherent laser pulse,

$$H_{\mathrm{QD-L}} = \sum_{i=H,V} ((|G\rangle\langle X_i|\Omega_i^*(t) + |X_i\rangle\langle B|\Omega_i^*(t)) + \mathrm{H.c.}), \quad \text{(A4)}$$

with Rabi frequency Ω_i. Here we assume zero fine-structure splitting for the excitons with δ_{fss}. In this case, we can simplify the following analysis by assuming circular polarization of the control laser. The desired single-photon emission can then be detected in the other circular polarization channel as sketched in Fig. 1. In the circularly polarized frame, the coherent light field and cavity photon operators take the following form:

$$\Omega_{\sigma^\pm}^* = \frac{1}{\sqrt{2}}(\Omega_H^* \pm \mathrm{i}\Omega_V^*) \text{ and } b_{\sigma^\pm}^\dagger = \frac{1}{\sqrt{2}}(b_H^\dagger \pm \mathrm{i}b_V^\dagger) \quad \text{(A5)}$$

We solve the equations of motion in the linear basis with a circularly polarized driving pulse and from this obtain the corresponding circularly polarized photons as stated above. However, for the analytical rates derived in Sec. III A, the Hamiltonian in the circular basis is conveniently used instead. The exciton states in the circular basis are given by $|X_{\sigma^\pm}\rangle = \frac{1}{\sqrt{2}}(|X_H\rangle \pm \mathrm{i}|X_V\rangle)$. Together, the full Hamiltonian of the light matter interaction in the circular basis then reads

$$H_{\mathrm{int}} = (|G\rangle\langle X_{\sigma^+}| + |X_{\sigma^-}\rangle\langle B|)(gb_{\sigma^+}^\dagger + \Omega_{\sigma^+}^*(t)) + \mathrm{H.c.} + (|G\rangle\langle X_{\sigma^-}| + |X_{\sigma^+}\rangle\langle B|)(gb_{\sigma^-}^\dagger + \Omega_{\sigma^-}^*(t)) + \mathrm{H.c.} \quad \text{(A6)}$$

The relevant equations of motion in the polaron frame will be formulated in the following sections.

b. Phonon part

In the case of InAs/GaAs QDs driven near resonance, the interaction with phonons is predominantly governed by the coupling to LA phonons [50]. By modeling the phonon bath as harmonic oscillators with wave vector $\boldsymbol{q}$ and energy $\hbar\omega_{\boldsymbol{q}}$, the Hamiltonian of the phonon bath may be written as [31,54]

$$H_{\mathrm{B}} = \sum_{\boldsymbol{q}} \hbar\omega_{\boldsymbol{q}} a_{\boldsymbol{q}}^\dagger a_{\boldsymbol{q}}, \quad \text{(A7)}$$

while

$$H_{\mathrm{QD-Ph}} = \sum_{s=B,X_{\mathrm{H}},X_{\mathrm{V}}} |s\rangle\langle s| \sum_{\boldsymbol{q}} \hbar\lambda_{\boldsymbol{q}}^i (a_{\boldsymbol{q}}^\dagger + a_{\boldsymbol{q}}) \quad \text{(A8)}$$

describes the electron-phonon interaction. Here, $a_{\boldsymbol{q}}^\dagger$ and $a_{\boldsymbol{q}}$ are bosonic creation and annihilation operators for a phonon in mode $\boldsymbol{q}$. The exciton-phonon coupling strength can be quantified by real constants $\lambda_{\boldsymbol{q}}^i$ [30,55]. Furthermore, for an ideal QD we have $\lambda_{\boldsymbol{q}}^B = 2\lambda_{\boldsymbol{q}}^{X_{\mathrm{H}}} = 2\lambda_{\boldsymbol{q}}^{X_{\mathrm{V}}}$ [56].

c. Polaron transformation

At this point, a commonly used approach [30,31] is to apply the transformation

$$H' = e^S H e^{-S} \quad \text{with } S = \sum_{s=B,X_{\mathrm{H}},X_{\mathrm{V}}} |s\rangle\langle s| \sum_{\boldsymbol{q}} \frac{\lambda_{\boldsymbol{q}}^s}{\omega_{\boldsymbol{q}}} (a_{\boldsymbol{q}}^\dagger - a_{\boldsymbol{q}}). \quad \text{(A9)}$$

This transforms the Hamiltonian into the polaron frame, removing the explicit appearance of the electron-phonon interaction $H_{\mathrm{QD-Ph}}$ [57,58]. Using the Baker-Campbell-Hausdorff formula the transformation defined by Eq. (A9) may be carried out analytically [55], yielding

$$H' = H_0' + H_S' + H_{\mathrm{B}} + H_{\mathrm{I}}. \quad \text{(A10)}$$

Here, the transformed Hamiltonian of the QD and the cavity modes is given by

$$H_0' = \sum_{s=B,G,X_{\mathrm{H}},X_{\mathrm{V}}} E_s'|s\rangle\langle s| + \sum_{i=\mathrm{H,V}} \hbar\omega_{\mathrm{c}} b_j^\dagger b_j, \quad \text{(A11)}$$

where $E_s' = E_s - \sum_{\boldsymbol{q}} \lambda_{\boldsymbol{q}}^s/\omega_{\boldsymbol{q}}$. This polaron shift of the QD energy levels can be included in the original definition of E_s and therefore be disregarded [30]. The transformed QD interaction Hamiltonian

$$H_S' = \langle B\rangle H_S \quad \text{(A12)}$$

is scaled by the thermal average of the phonon bath displacement operator [50]. Since $\langle B\rangle < 1$, this effectively decreases the coupling strengths g and $\Omega(t)$. Lastly, the new interaction Hamiltonian of the phonon–assisted optical transitions is given by

$$H_I = \zeta_g X_g - \zeta_u X_u, \quad \text{(A13)}$$

with fluctuation operators $\zeta_g = \frac{1}{2}(B_+ + B_- - 2\langle B\rangle)$ and $\zeta_u = B_+ + B_-$ [58] which are Hermitian combinations of the otherwise non-Hermitian operators $B_\pm$ [59].

2. System dynamics

The density matrix ρ of the quantum-dot cavity system in the polaron frame obeys the following Liouville-von Neuman equation [15,30,58]:

$$\frac{d}{d\mathrm{t}}\rho(t) = \frac{1}{\mathrm{i}\hbar}[H_S'(t), \rho] + \mathcal{L}_{\mathrm{cav}}(\rho) + \mathcal{L}_{\mathrm{pure}}(\rho) + \mathcal{L}_{\mathrm{phonon}}(\rho) + \mathcal{L}_{\mathrm{rad}}'(\rho), \quad \text{(A14)}$$

which includes coupling to an environment via contributions of the type $\mathcal{L}(\rho)$. The loss of cavity photons is included by

$$\mathcal{L}_{\mathrm{cavity}}(\rho_s) = \frac{\kappa}{2\hbar} \sum_{i=H,V} (2b_i\rho_s b_i^\dagger - b_i^\dagger b_i\rho_s - \rho_s b_i^\dagger b_i), \quad \text{(A15)}$$

where κ is the cavity loss rate which is varied in fractions/multiples of g to investigate both weak and strong coupling. We use $g = \hbar/10\ \mathrm{ps}^{-1}$, $g/\kappa = 0.35$, and a biexciton binding energy of 3 meV if no other values are stated. To

account for the decay of quantum-dot coherences, a pure dephasing term

$$\mathcal{L}_{\text{pure}}(\rho_s) = \frac{1}{2\hbar} \sum_{\chi,\chi':\chi\neq\chi'} \gamma_{\text{pure}}^{\chi,\chi'} |\chi\rangle\langle\chi|\rho_s|\chi'\rangle\langle\chi'|, \tag{A16}$$

with $\chi, \chi' \in \{G, X_H, X_V, B\}$ is included. A linear increase of the pure dephasing rate γ_{pure} at low temperatures T is accounted for as $\gamma_{\text{pure}}(T) = {}^{1\mu\text{eV}}/_{K} \times T$ [31,32]. Additionally, phonon-assisted optical transitions are included using a second-order Born-Markov approximation tracing out the phononic degrees of freedom. The term obtained describing the electron-phonon interaction reads [30,55]

$$\mathcal{L}_{\text{phonon}}(\rho) = -\frac{1}{\hbar^2}\int_0^\infty d\tau \times \sum_{m=g,u} (G_m(\tau)[X_m(t), X_m(t-\tau,t)\rho(t)] + \text{H.c.}), \tag{A17}$$

and captures phonon-assisted optical transitions as well as energy shifts related to the coupling to the phonon bath. Equation (A17) is found to be a valid approximation if [30,60]

$$\Pi := \left(\frac{\Xi}{\omega_b}\right)^2 (1 - \langle B\rangle^4) \ll 1. \tag{A18}$$

Here, Ξ is either the coupling of electronic states to the cavity modes for which the above relation is clearly fulfilled or the coupling to the laser pulse for which we limit the pulse intensity accordingly to $\Pi < 0.1$.

The polaron Green functions are given by [31]

$$G_g(\tau) = \langle B\rangle^2(\cosh(\phi(\tau)) - 1), \tag{A19}$$

$$G_u(\tau) = \langle B\rangle^2 \sinh(\phi(\tau)), \tag{A20}$$

with the phonon correlation function [57,58]

$$\phi(t) = \int_0^\infty \frac{J(\omega)}{\omega^2}\left[\coth\left(\frac{\hbar\omega}{2k_BT}\right)\cos(\omega\tau) - \text{i}\sin(\omega\tau)\right]d\omega \tag{A21}$$

and the thermal average of the phonon bath displacement operator [50]

$$\langle B\rangle \equiv \langle B_\pm\rangle = \exp\left[-\frac{1}{2}\int_0^\infty \frac{J(\omega)}{\omega^2}\coth\left(\frac{\hbar\omega}{2k_BT}\right)d\omega\right], \tag{A22}$$

where T is the temperature of the QD sample. The main source of phonon-induced dephasing in InAs/GaAs QDs is a deformation potential induced by LA phonons [50,61,62]. In this case, the phonon spectral function may be written as

$$J(\omega) = \alpha\omega^3 e^{-\frac{\omega^2}{2\omega_b^2}}, \tag{A23}$$

where exciton-phonon coupling strength α and phonon cutoff frequency ω_b are material parameters of the QD. Typical experimental values in InAs/GaAs QDs are $\alpha = 0.03$ ps^2 and $\hbar\omega_b = 1$ meV [55]. The phonon-assisted operators are

$$X_g = \mathcal{X} + \text{H.c.} \quad \text{and} \quad X_u = \text{i}(\mathcal{X} - \text{H.c.}), \tag{A24}$$

where

$$\mathcal{X} = \sum_{j=\text{H,V}} (|X_j\rangle\langle G| + |B\rangle\langle X_j|)(gb_j + \Omega_j). \tag{A25}$$

We note that in the numerical implementation, all operators are treated in the interaction picture with respect to H_0 [16].

The optical quantum–dot transitions are time-dependent in the interaction picture $X_m(t-\tau,t)$. To calculate the $X_m(t-\tau,t)$ exactly, we resort to solving the Heisenberg equation of motion [55],

$$\frac{d}{d\tau}O(t-\tau) = \frac{1}{\text{i}\hbar}[H_I'(t-\tau), O(t-\tau)] + \frac{\partial}{\partial\tau}O(t-\tau), \tag{A26}$$

with $O(t-\tau) \in \{|X_j\rangle\langle G|b_j, |B\rangle\langle X_j|b_j, |X_j\rangle\langle G|\Omega(t-\tau), |B\rangle\langle X_j|\Omega(t-\tau)\}$. Integrating this differential equation from the initial condition $O(t-0,t) = O(t)$ backward until $t-\tau$ yields $O(t-\tau,t)$ and thus $X_m(t-\tau,t)$ via Eqs. (A24) and (A25). Note that in the interaction picture, the involved operators carry an explicit time dependence, for instance,

$$\frac{\partial}{\partial\tau}[|X_j\rangle\langle G|b_j(t-\tau)] = -\text{i}(\omega_{X_j} - \omega_G - \omega_c)|X_j\rangle\langle G|b_j(t-\tau). \tag{A27}$$

We also consider radiative decay into modes other than the system cavity modes with [12,31,50]

$$\mathcal{L}_{\text{rad}}(\rho_s) = \frac{\gamma_{\text{rad}}}{\hbar}\sum_{i=X_H,X_V}(\mathcal{L}_{|G\rangle\langle i|} + \mathcal{L}_{|i\rangle\langle B|})(\rho_s), \tag{A28}$$

where we chose $\gamma_{\text{rad}} = 2$ μeV and

$$\mathcal{L}_\sigma(\rho_s) = (2\sigma\rho_s\sigma^\dagger - \sigma^\dagger\sigma\rho_s - \rho_s\sigma^\dagger\sigma). \tag{A29}$$

The polaron-transformed Hamiltonian H_S' [Eq. (A10)] which appears in the polaron master equation for the density matrix ρ scales the optical transitions in H_S [63] by a factor of $\langle B\rangle$. This rescaling also occurs in the radiative decay term with $\mathcal{L}_{\text{rad}}'(\rho) = \langle B\rangle^2\mathcal{L}_{\text{rad}}(\rho)$ [50,58].

3. Single photon properties

In this section, we introduce the photon emission spectrum as well as the indistinguishability and purity.

a. Single photon emission spectrum

In Fig. 1(d), we introduced the cavity emission spectrum, which is known as the physical spectrum of light [12,16,64]. It can be calculated as

$$S_i(\mathcal{T},\omega) = \Re\int_0^{\mathcal{T}} dt \int_0^{\mathcal{T}-t} d\tau\, \langle b_i^\dagger(t)b_i(t+\tau)\rangle e^{i\omega\tau} \tag{A30}$$

for a given (circular) polarization i up to a time $\mathcal{T}$ and it requires the evaluation of two-time expectation values which we calculate using the quantum regression theorem [65]. We note that in the cases considered here, the single-photon emission process is completed in a time frame less than 60 ps such that we can safely chose $\mathcal{T} = 60$ ps as a cutoff value for the time integrations.

TABLE I. List of parameters of those pulses for which optimal emissions are found as shown in Fig. 5 (initial condition $|B\rangle$) and Fig. 6 (initial condition $|G\rangle$) for $\mathcal{E}_0 = 3$ at different temperatures.

Initial condition	$\|G\rangle$	$\|G\rangle$	$\|B\rangle$	$\|B\rangle$
T [K]	1	4	1	4
Δ_L [meV]	0.17	0.17	0.16	0.15
α [rad]	2.05	3.14	3.14	3.14
γ [meV^{-1}]	1.31	1.14	1.13	1.17
δ [rad]	2.69	2.72	−0.74	−0.74
η [meV^{-2}]	12.94	0.80	−25.0	−24.44
t_0 [ps]	26.75	25.56	22.38	22.73
σ [ps]	4.97	5.0	5.0	4.99
Pulse area [π]	8.2	8.2	8.1	8.2

b. Indistinguishability and purity

The purity and indistinguishability of an emitted photon are crucial figures of merit of single-photon sources. Those properties are essential for applications of quantum technology [66]. The single-photon purity quantifies whether a quantum light field contains more than one photon. It is defined as the normalized equal-time two-photon expectation value [67]:

$$g_i^{(2)}(0) = \frac{\langle b_i^\dagger(t) b_i^\dagger(t) b_i(t) b_i(t)\rangle}{\langle b_i^\dagger(t) b_i(t)\rangle^2}. \tag{A31}$$

The two-photon component of a pure single-photon field equals zero.

The indistinguishability is of importance whenever photon-photon interaction is vital [66]. It can be measured in a Hong-Ou-Mandel interference experiment and reflects the joint detection probability at two photon detectors [68]. We model this coincidence detection probability according to Ref. [55] as

$$p_c = \frac{\int_0^{\mathcal{T}} \int_0^{\mathcal{T}} G^{(2)}_{\mathrm{HOM},i}(t,\tau)\, d\tau\, dt}{\int_0^{\mathcal{T}} \int_0^{\mathcal{T}} \left(2G^{(2)}_{\mathrm{pop},i}(t,\tau) - |\langle b_i(t+\tau)\rangle\langle b_i^\dagger(t)\rangle|^2\right) d\tau\, dt}. \tag{A32}$$

Here

$$G^{(2)}_{\mathrm{HOM},i}(t,\tau) = \tfrac{1}{2}\big(G^{(2)}_{\mathrm{pop},i}(t,\tau) + G^{(2)}_i(t,\tau) - |\langle b_i^\dagger(t+\tau) b_i(t)\rangle|^2\big), \tag{A33}$$

with $G^{(2)}_{\mathrm{pop},i}(t,\tau) = \langle b_i^\dagger b_i\rangle(t)\langle b_i^\dagger b_i\rangle(t+\tau)$ and $G^{(2)}_i(t,\tau) = \langle b_i^\dagger(t) b_i^\dagger(t+\tau) b_i(t+\tau) b_i(t)\rangle$ is the second-order autocorrelation function. The indistinguishability $\mathcal{I} = 1 - p_c$ has a maximal value of 1.

APPENDIX B: OPTIMIZED PULSES

Table I lists sets of parameters for which an optimal emission was found as shown in Figs. 5 and 6 for $\mathcal{E}_0 = 3$ at different temperatures. Either an initially prepared biexciton state is assumed (system initially in state $|B\rangle$ with zero photons) or the biexciton state is prepared by two-photon absorption from the ground state of the quantum dot (system initially in state $|G\rangle$ with zero photons). We note that an initialization pulse may also introduce pulse-dependent spectral shifts, which are reflected in the optimized parameters of the (temporally overlapping) control pulse.

[1] E. Knill, R. Laflamme, and G. J. Milburn, A scheme for efficient quantum computation with linear optics, Nature (London) **409**, 46 (2001).

[2] N. Gisin, G. Ribordy, W. Tittel, and H. Zbinden, Quantum cryptography, Rev. Mod. Phys. **74**, 145 (2002).

[3] X. Ding, Y. He, Z.-C. Duan, N. Gregersen, M.-C. Chen, S. Unsleber, S. Maier, C. Schneider, M. Kamp, S. Höfling, C.-Y. Lu, and J.-W. Pan, On-Demand Single Photons with High Extraction Efficiency and Near-Unity Indistinguishability from a Resonantly Driven Quantum Dot in a Micropillar, Phys. Rev. Lett. **116**, 020401 (2016).

[4] L. Hanschke, K. A. Fischer, S. Appel, D. Lukin, J. Wierzbowski, S. Sun, R. Trivedi, J. Vučković, J. J. Finley, and K. Müller, Quantum dot single-photon sources with ultra-low multi-photon probability, npj Quantum Inf. **4**, 43 (2018).

[5] Y. Chen, M. Zopf, R. Keil, F. Ding, and O. G. Schmidt, Highly-efficient extraction of entangled photons from quantum dots using a broadband optical antenna, Nat. Commun. **9**, 2994 (2018).

[6] D. Huber, M. Reindl, S. F. Covre da Silva, C. Schimpf, J. Martín-Sánchez, H. Huang, G. Piredda, J. Edlinger, A. Rastelli, and R. Trotta, Strain-Tunable GaAs Quantum dot: A Nearly Dephasing-Free Source of Entangled Photon Pairs on Demand, Phys. Rev. Lett. **121**, 033902 (2018).

[7] J. Liu, R. Su, Y. Wei, B. Yao, S. F. C. d. Silva, Y. Yu, J. Iles-Smith, K. Srinivasan, A. Rastelli, J. Li, and X. Wang, A solid-state source of strongly entangled photon pairs with high brightness and indistinguishability, Nat. Nanotechnol. **14**, 586 (2019).

[8] H. Wang, H. Hu, T.-H. Chung, J. Qin, X. Yang, J.-P. Li, R.-Z. Liu, H.-S. Zhong, Y.-M. He, X. Ding, Y.-H. Deng, Q. Dai, Y.-H. Huo, S. Höfling, C.-Y. Lu, and J.-W. Pan, On-Demand Semiconductor Source of Entangled Photons Which Simultaneously has High Fidelity, Efficiency, and Indistinguishability, Phys. Rev. Lett. **122**, 113602 (2019).

[9] D. Bauch, D. Heinze, J. Förstner, K. D. Jöns, and S. Schumacher, Ultrafast electric control of cavity mediated single-photon and photon-pair generation with semiconductor quantum dots, Phys. Rev. B **104**, 085308 (2021).

[10] S. Stufler, P. Machnikowski, P. Ester, M. Bichler, V. M. Axt, T. Kuhn, and A. Zrenner, Two-photon Rabi oscillations in a single In_x Ga_{1-x} As/GaAs quantum dot, Phys. Rev. B **73**, 125304 (2006).

[11] S. Bounouar, M. Müller, A. M. Barth, M. Glässl, V. M. Axt, and P. Michler, Phonon-assisted robust and deterministic two-photon biexciton preparation in a quantum dot, Phys. Rev. B **91**, 161302(R) (2015).

[12] E. Del Valle, A. Gonzalez-Tudela, E. Cancellieri, F. Laussy, and C. Tejedor, Generation of a two-photon state from a quantum dot in a microcavity, New J. Phys. **13**, 113014 (2011).

[13] Y. Ota, S. Iwamoto, N. Kumagai, and Y. Arakawa, Spontaneous Two-Photon Emission from a Single Quantum Dot, Phys. Rev. Lett. **107**, 233602 (2011).

[14] S. Schumacher, J. Förstner, A. Zrenner, M. Florian, C. Gies, P. Gartner, and F. Jahnke, Cavity-assisted emission of polarization-entangled photons from biexcitons in quantum dots with fine-structure splitting, Opt. Express **20**, 5335 (2012).

[15] D. Heinze, D. Breddermann, A. Zrenner, and S. Schumacher, A quantum dot single-photon source with on-the-fly all-optical polarization control and timed emission, Nat. Commun. **6**, 8473 (2015).

[16] D. Breddermann, D. Heinze, R. Binder, A. Zrenner, and S. Schumacher, All-optical tailoring of single-photon spectra in a quantum-dot microcavity system, Phys. Rev. B **94**, 165310 (2016).

[17] S. Thomas and P. Senellart, The race for the ideal single-photon source is on, Nat. Nanotechnol. **16**, 367 (2021).

[18] B. Jonas, D. Heinze, E. Schöll, P. Kallert, T. Langer, S. Krehs, A. Widhalm, K. D. Jöns, D. Reuter, S. Schumacher, and A. Zrenner, Nonlinear down-conversion in a single quantum dot, arXiv:2105.12393.

[19] M. Atatüre, J. Dreiser, A. Badolato, A. Högele, K. Karrai, and A. Imamoglu, Quantum-dot spin-state preparation with near-unity fidelity, Science **312**, 551 (2006).

[20] C. Santori, D. Fattal, K.-M. C. Fu, P. E. Barclay, and R. G. Beausoleil, On the indistinguishability of Raman photons, New J. Phys. **11**, 123009 (2009).

[21] T. M. Sweeney, S. G. Carter, A. S. Bracker, M. Kim, C. S. Kim, L. Yang, P. M. Vora, P. G. Brereton, E. R. Cleveland, and D. Gammon, Cavity-stimulated Raman emission from a single quantum dot spin, Nat. Photonics **8**, 442 (2014).

[22] P. M. Vora, A. S. Bracker, S. G. Carter, T. M. Sweeney, M. Kim, C. S. Kim, L. Yang, P. G. Brereton, S. E. Economou, and D. Gammon, Spin-cavity interactions between a quantum dot molecule and a photonic crystal cavity, Nat. Commun. **6**, 7665 (2015).

[23] D. Breddermann, T. Praschan, D. Heinze, R. Binder, and S. Schumacher, Microscopic theory of cavity-enhanced single-photon emission from optical two-photon Raman processes, Phys. Rev. B **97**, 125303 (2018).

[24] M. Varnava, D. E. Browne, and T. Rudolph, How Good Must Single Photon Sources and Detectors be for Efficient Linear Optical Quantum Computation? Phys. Rev. Lett. **100**, 060502 (2008).

[25] A. Neville, C. Sparrow, R. Clifford, E. Johnston, P. M. Birchall, A. Montanaro, and A. Laing, Classical boson sampling algorithms with superior performance to near-term experiments, Nat. Phys. **13**, 1153 (2017).

[26] R. J. Young, R. M. Stevenson, A. J. Shields, P. Atkinson, K. Cooper, D. A. Ritchie, K. M. Groom, A. I. Tartakovskii, and M. S. Skolnick, Inversion of exciton level splitting in quantum dots, Phys. Rev. B **72**, 113305 (2005).

[27] M. Cygorek, M. Cosacchi, A. Vagov, V. M. Axt, B. W. Lovett, J. Keeling, and E. M. Gauger, Numerically-exact simulations of arbitrary open quantum systems using automated compression of environments, arXiv:2101.01653.

[28] M. Cygorek, A. M. Barth, F. Ungar, A. Vagov, and V. M. Axt, Nonlinear cavity feeding and unconventional photon statistics in solid-state cavity QED revealed by many-level real-time path-integral calculations, Phys. Rev. B **96**, 201201(R) (2017).

[29] A. Strathearn, P. Kirton, D. Kilda, J. Keeling, and B. W. Lovett, Efficient non-Markovian quantum dynamics using time-evolving matrix product operators, Nat. Commun. **9**, 3322 (2018).

[30] R. Manson, K. Roy-Choudhury, and S. Hughes, Polaron master equation theory of pulse-driven phonon-assisted population inversion and single-photon emission from quantum-dot excitons, Phys. Rev. B **93**, 155423 (2016).

[31] C. Roy and S. Hughes, Polaron master equation theory of the quantum-dot Mollow triplet in a semiconductor cavity-QED system, Phys. Rev. B **85**, 115309 (2012).

[32] A. Laucht, N. Hauke, J. M. Villas-Bôas, F. Hofbauer, G. Böhm, M. Kaniber, and J. J. Finley, Dephasing of Exciton Polaritons in Photoexcited InGaAs Quantum Dots in GaAs Nanocavities, Phys. Rev. Lett. **103**, 087405 (2009).

[33] P. K. Pathak and S. Hughes, Coherently triggered single photons from a quantum-dot cavity system, Phys. Rev. B **82**, 045308 (2010).

[34] P. Kumar and A. G. Vedeshwar, Phonon-assisted control of the single-photon spectral characteristics in a semiconductor quantum dot using cavity-assisted adiabatic passage, Phys. Rev. A **96**, 033808 (2017).

[35] B. J. Sussman, R. Lausten, and A. Stolow, Focusing of light following a 4-f pulse shaper: Considerations for quantum control, Phys. Rev. A **77**, 043416 (2008).

[36] A. Debnath, C. Meier, B. Chatel, and T. Amand, Chirped laser excitation of quantum dot excitons coupled to a phonon bath, Phys. Rev. B **86**, 161304(R) (2012).

[37] R. Mathew, Hong Yi Shi Yang, and K. C. Hall, Simultaneous SU(2) rotations on multiple quantum dot exciton qubits using a single shaped pulse, Phys. Rev. B **92**, 155306 (2015).

[38] V. S. Malinovsky and J. L. Krause, General theory of population transfer by adiabatic rapid passage with intense, chirped laser pulses, Eur. Phys. J. D **14**, 147 (2001).

[39] I. Griva, S. G. Nash, and A. Sofer, *Linear and Nonlinear Optimization*, 2nd ed. (SIAM, Philadelphia, PA, 2009), Vol. 108.

[40] M. Glässl, A. M. Barth, K. Gawarecki, P. Machnikowski, M. D. Croitoru, S. Lüker, D. E. Reiter, T. Kuhn, and V. M. Axt, Biexciton state preparation in a quantum dot via adiabatic rapid passage: Comparison between two control protocols and impact of phonon-induced dephasing, Phys. Rev. B **87**, 085303 (2013).

[41] R. Mathew, C. E. Pryor, M. E. Flatté, and K. C. Hall, Optimal quantum control for conditional rotation of exciton qubits in semiconductor quantum dots, Phys. Rev. B **84**, 205322 (2011).

[42] A. Wächter and L. T. Biegler, On the implementation of an interior-point filter line-search algorithm for large-scale nonlinear programming, Math. Program. **106**, 25 (2006).

[43] A. Wächter, Short tutorial: Getting started with IPOPT in 90 minutes, in *Dagstuhl Seminar Proceedings* (Schloss Dagstuhl – Leibniz Center for Informatics, Dagstuhl, Germany, 2009).

[44] R. Byrd, J. Gilbert, and J. Nocedal, A trust region method based on interior point techniques for nonlinear programming, Math. Program. **89**, 149 (2000).

[45] M. Bartholomew-Biggs, S. Brown, B. Christianson, and L. Dixon, Automatic differentiation of algorithms, J. Comput. Appl. Math. **124**, 171 (2000), Numerical Analysis 2000. Vol. IV: Optimization and Nonlinear Equations.

[46] A. Walther and A. Griewank, Getting started with ADOL-C, in *Combinatorial Scientific Computing* (Schloss Dagstuhl – Leibniz-Zentrum fuer Informatik (English Schloss Dagstuhl – Leibniz Center for Informatics, Dagstuhl, Germany, 2009), Vol. 09061, pp. 181–202.

[47] A. Griewank and A. Walther, *Evaluating Derivatives: Principles and Techniques of Algorithmic Differentiation*, 2nd ed. (SIAM, Philadelphia, PA, 2008).

[48] A. Kowarz and A. Walther, Optimal checkpointing for time-stepping procedures in ADOL-C, in *International Conference on Computational Science* (Springer, Berlin, Heidelberg, 2006), pp. 541–549.

[49] M. Sagebaum, T. Albring, and N. R. Gauger, High-performance derivative computations using CoDiPack, ACM Trans. Math. Softw. **45**, 26 (2019).

[50] C. Roy and S. Hughes, Influence of Electron–Acoustic-Phonon Scattering on Intensity Power Broadening in a Coherently Driven Quantum-Dot–Cavity System, Phys. Rev. X **1**, 021009 (2011).

[51] P.-L. Ardelt, L. Hanschke, K. A. Fischer, K. Müller, A. Kleinkauf, M. Koller, A. Bechtold, T. Simmet, J. Wierzbowski, H. Riedl, G. Abstreiter, and J. J. Finley, Dissipative preparation of the exciton and biexciton in self-assembled quantum dots on picosecond time scales, Phys. Rev. B **90**, 241404(R) (2014).

[52] J. H. Quilter, A. J. Brash, F. Liu, M. Glässl, A. M. Barth, V. M. Axt, A. J. Ramsay, M. S. Skolnick, and A. M. Fox, Phonon-Assisted Population Inversion of a Single InGaAs/GaAs Quantum Dot by Pulsed Laser Excitation, Phys. Rev. Lett. **114**, 137401 (2015).

[53] S. Lüker and D. E. Reiter, A review on optical excitation of semiconductor quantum dots under the influence of phonons, Semicond. Sci. Technol. **34**, 063002 (2019).

[54] F. Hargart, M. Müller, K. Roy-Choudhury, S. L. Portalupi, C. Schneider, S. Höfling, M. Kamp, S. Hughes, and P. Michler, Cavity-enhanced simultaneous dressing of quantum dot exciton and biexciton states, Phys. Rev. B **93**, 115308 (2016).

[55] C. Gustin and S. Hughes, Pulsed excitation dynamics in quantum-dot–cavity systems: Limits to optimizing the fidelity of on-demand single-photon sources, Phys. Rev. B **98**, 045309 (2018).

[56] U. Hohenester, G. Pfanner, and M. Seliger, Phonon-Assisted Decoherence in the Production of Polarization-Entangled Photons in a Single Semiconductor Quantum Dot, Phys. Rev. Lett. **99**, 047402 (2007).

[57] I. Wilson-Rae and A. Imamoğlu, Quantum dot cavity-QED in the presence of strong electron-phonon interactions, Phys. Rev. B **65**, 235311 (2002).

[58] D. Heinze, A. Zrenner, and S. Schumacher, Polarization-entangled twin photons from two-photon quantum-dot emission, Phys. Rev. B **95**, 245306 (2017).

[59] A. Würger, Strong-coupling theory for the spin-phonon model, Phys. Rev. B **57**, 347 (1998).

[60] D. P. S. McCutcheon and A. Nazir, Quantum dot Rabi rotations beyond the weak exciton–phonon coupling regime, New J. Phys. **12**, 113042 (2010).

[61] A. J. Ramsay, A. V. Gopal, E. M. Gauger, A. Nazir, B. W. Lovett, A. M. Fox, and M. S. Skolnick, Damping of Exciton Rabi Rotations by Acoustic Phonons in Optically Excited InGaAs/GaAs Quantum Dots, Phys. Rev. Lett. **104**, 017402 (2010).

[62] B. Krummheuer, V. M. Axt, and T. Kuhn, Theory of pure dephasing and the resulting absorption line shape in semiconductor quantum dots, Phys. Rev. B **65**, 195313 (2002).

[63] A. Krügel, V. M. Axt, T. Kuhn, P. Machnikowski, and A. Vagov, The role of acoustic phonons for Rabi oscillations in semiconductor quantum dots, Appl. Phys. B **81**, 897 (2005).

[64] J. H. Eberly and K. Wódkiewicz, The time-dependent physical spectrum of light, J. Opt. Soc. Am. **67**, 1252 (1977).

[65] H. J. Carmichael, *Statistical Methods in Quantum Optics 1*, corrected second printing ed. (Berlin, Heidelberg: Springer-Verlag, 1999).

[66] P. Senellart, G. Solomon, and A. White, High-performance semiconductor quantum-dot single-photon sources, Nat. Nanotechnol. **12**, 1026 (2017).

[67] M. Fox, *Quantum Optics: An Introduction*, Oxford Master Series in Physics (Oxford University Press, Oxford, 2006).

[68] C. K. Hong, Z. Y. Ou, and L. Mandel, Measurement of Subpicosecond Time Intervals Between Two Photons by Interference, Phys. Rev. Lett. **59**, 2044 (1987).